Strain-Induced Changes of Free Volume Measured by Positron Lifetime Spectroscopy in Ultrahigh Molecular Weight Polyethylene

M. A. Monge,* J. A. Díaz, and R. Pareja

Departamento de Física, Universidad Carlos III de Madrid, 28911 Leganés, Spain

Received May 7, 2004; Revised Manuscript Received July 8, 2004

ABSTRACT: Positron lifetime spectroscopy and wide-angle X-ray scattering have been applied to investigate the structural changes induced by tensile deformation in ultrahigh molecular weight linear polyethylene. The results reveal a correlation between the crystallinity, the positron annihilation characteristics, and the strain of the polymer. The probability of positronium formation increases and the crystallinity of the material decreases with increasing tensile strain. The size distribution of the free-volume holes, where positronium atoms form, is determined from their lifetime distribution. The positron lifetime measurements are interpreted in terms of a free-volume approach assuming that the free volume associated with each liquidlike cell of the amorphous phase is divided into free-volume holes whose size distribution is given by a normal frequency function. The cumulative distribution functions determined from the positron annihilation measurements agrees with those predicted by the free-volume model. This indicates that the positrons contributing to the lifetime component associated with orthopositronium annihilation really probe the free volume in the amorphous phase of the polymer. The experiments evidence free-volume changes induced by tensile strain which are unrecoverable after relieving the stress.

1. Introduction

It is well-known that deformation transforms the isotropic spherulitic structure of a semicrystalline polymer into an anisotropic microfibrillar structure. This transformation produces remarkable changes in its mechanical properties. Thus, to understand this transformation is of technological and scientific interest. Recently, the deformation behavior for an ample variety of semicrystalline polymers has been investigated under true strain-controlled tensile tests. The true stress−strain curves show three well-defined points with constant strain values, stress independent, where the differential compliance, the recovery properties, and the crystalline texture of the polymer change simultaneously.[1−4] This appears to be a general behavior independent of crystallinity for polyethylene (PE), syndiotatic polypropylene (s-PP), isotactic poly(1-butene) (P1B), and some of their copolymers. These critical points are correlated with qualitative changes in the deformation mechanism. They successively correspond with (A) the onset of isolated inter- and intralamellar slip processes, (B) a transition to collective shear processes, and (C) the starting of the crystalline fragmentation. A four point (D), whose critical strain is temperature dependent, is associated with chain disentanglement inducing true plastic deformation. There are other many reports describing the deformation mechanism of linear high-density polyethylene (HDPE) in similar terms of crystalline texture changes, inter- and intralamellar slip processes, and orientation changes of the chains in the amorphous phase.[5−7]

Other structure-sensitive properties of the semicrystalline polymers, such as gas diffusivity and permeability and mechanical relaxation, are successfully interpreted in terms of the free-volume concept.[8−16] Thus, free volume is considered as an intrinsic parameter that can control structural changes, relaxation processes, and transport phenomena in polymers. The free volume is defined as the difference between the total volume and the hypothetical volume occupied by the polymer molecules. One would expect changes in the free volume of a polymer after being plastically deformed. However, few reports are found showing evidence for such changes. For instance, a decrease of the fractional free volume in the amorphous phase has been reported in HDPE uniaxially drawn at 60 and 80 °C.[8] This result differs from that obtained by Galenski et al.[5] in HDPE channel die compressed at 80 °C. In this case, the density of the polymer decreases with the compression ratio, suggesting an increase of the fractional free volume in the whole of the polymer. Also, positron annihilation evidence of free-volume increase induced by deformation has been reported for an amorphous polycarbonate under tensile strain.[17] It should be noted that there exist reports for HDPE[18] and polypropylene,[20] giving evidence for microvoid formation during deformation not attributable to necking. The reason for this shortage of reports correlating deformation and free volume could be the lack of straightforward and accurate methods to measure the fractional free volume in a sample.

Positron lifetime spectroscopy (PLS) is successfully applied to determine the characteristics of the free-volume holes in polymers. Thermalized positrons in a polymer have the capability to probe its free volume because they can be localized in nanovoids as a positronium atom (Ps) in an ortho state ($^3S_1$). The lifetime of the ortho-Ps (o-Ps) localized in a free-volume hole, τ_{o-Ps}, is related to the hole radius R by[20]

$$\tau_{o-Ps} = \frac{1}{2}\left[1 - \frac{R}{R+\Delta R} + \frac{1}{2\pi}\sin\left(\frac{2\pi R}{R+\Delta R}\right)\right]^{-1} \quad (1)$$

where τ_{o-Ps} is given in nanoseconds and ΔR is the thickness of a homogeneous electron layer surrounding the free-volume hole where the Ps annihilates, so that $R_0 = R + \Delta R$ is the radius of the spherical potential

* Corresponding author. E-mail: mmonge@fis.uc3m.es.

10.1021/ma049103i CCC: $27.50
Published on Web 08/24/2004

wells corresponding to the free-volume hole. $\Delta R = 0.166$ nm is usually assumed for polymers according to experimental results in zeolites and molecular solids.[20] Thus, the τ_{o-Ps} value gives us an indication of the free volume hole size. The spectral intensity, I_{o-Ps}, is related to the number of free volume hole sites yielding an o-Ps in the polymer.

The aim of this work is to investigate the variation of the fractional free volume induced by tensile deformation in ultrahigh molecular weight linear polyethylene (UHMW PE) using PLS.

2. Experimental Section

Dumbbell-shaped samples with a total length of 150 mm and gauge dimensions $60 \times 10 \times 5$ mm^3 were stamped from 5 mm thick compression-molded sheets of UHMW PE [$M_w = (3-6) \times 10^6$]. Each sample was uniaxially stretched to different final extensions at room temperature using a tensile stress machine at a constant cross-head rate of 25 mm/min. To follow the evolution of the crystallinity with deformation, wide-angle X-ray scattering (WAXS) measurements were performed on the deformed samples immediately after unloading. These were carried out on an X-Pert Philips diffractometer with Bragg−Brentano configuration using the Cu Kα radiation. The crystalline mass fraction was determined from the ratio of the area under the crystalline peaks to the total area over the angular range 10°−30° (2θ) following the procedure described in ref 21. After WAXS measurements and strain recovery on unloading for 24 h at room temperature, a pair of samples 12 $\times$ 12 mm^2 was cut from the central area of the gauge region of the deformed samples for positron annihilation experiments. These experiments were carried out using a ^{22}Na positron source, deposited on a thin foil of Kapton, and sandwiched between the pair of samples. The positron lifetime spectrum at room temperature was registered using a spectrometer with a time resolution of 240 ps. For each measurement, a lifetime spectrum with 10^7 accumulated counts was registered by addition of successive 10^6 counts spectra with an insignificant drift in the time zero. Radiation effects on the lifetime spectrum, attributable to the ^{22}Na source, should be meaningless because the 10^6 counts spectra successively collected are undistinguishable one another. Assuming that the real positron lifetime spectrum for a semicrystalline polymer is a continuous distribution of lifetime values τ, the observed spectrum would be

$$y(t) = R(t) \otimes [N_t s(t) + B] \quad (2)$$

where $\otimes$ represents the convolution of the resolution function of the spectrometer, $R(t)$, with the annihilation decay integral function, $s(t)$, and N_t and B are the total counts and the background of the spectrum, respectively. The function $s(t)$ is given by

$$s(t) = \int_0^\infty \frac{I(\tau)}{\tau} \exp\left(-\frac{t}{\tau}\right) d\tau = \int_0^\infty \lambda \alpha(\lambda) \exp(-\lambda t)\, d\lambda \quad (3)$$

where $\lambda = \tau^{-1}$ is the positron annihilation rate, $\alpha(\lambda)$ is the probability density function for a given annihilation rate, and $\int_0^\infty I(\tau)\, d\tau = \int_0^\infty \alpha(\lambda)\, d\lambda = 1$. The experimental spectra were analyzed with the MELT 4.0 routine[22] to obtain a continuous lifetime distribution. Also, discrete term fits of the spectra are performed using the routine PATFIT[23] in order to obtain reliable and accurate values for the input parameters required by MELT.

3. Results and Discussion

3.1. Applied Strain Effect on the WAXS Crystallinity. Figure 1 shows the engineering stress−extension curve and the corresponding true stress−true strain curve for a sample deformed up to a final extension $\epsilon = 3.5$. As true strain, we have taken the Hencky strain $\epsilon_H = \ln(1 + \epsilon)$. Applying the Considère construction on the true stress−extension curves, the yield point is determined at an applied extension of 0.26, corresponding to a yield stress of 25 MPa for all the samples. After a very small decrease of the hardening rate above the yield point, strain hardening appears at applied extension of ~1.2 going on up to fracture at ~4.0.

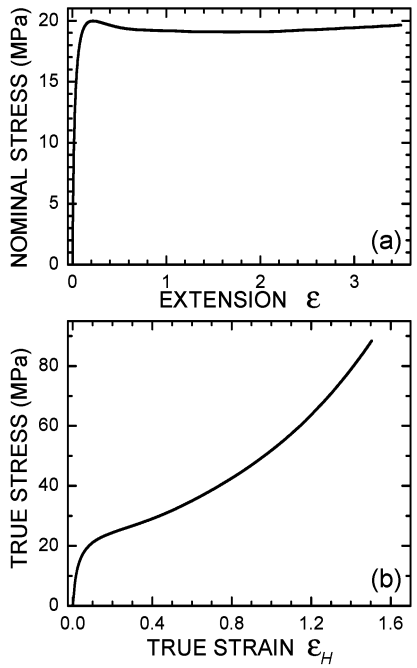

Figure 1. Typical stress−strain curve for UHMW PE tensile tested at a constant cross-head rate of 25 mm/min: (a) nominal stress−strain curve and (b) true stress−strain curve.

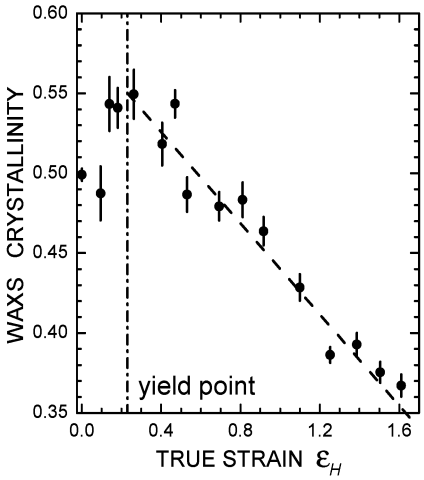

Figure 2. Crystalline fraction as a function of final applied strain for UHMW PE tensile tested.

The WAXS crystallinity varies with the final extension applied to the samples as Figure 2 shows. A small increase of the crystallinity appears to be produced when the samples are deformed up to around the yield point, i.e., at $\epsilon_H \cong 0.23$. Afterward, a continuous decrease is observed increasing strain up to fracture. The crystallinity decreases from 55% to 37%. This decrease is essentially linear with the true strain.

3.2. PLS Results and Determination of the Fractional Free Volume. The four discrete-term analyses

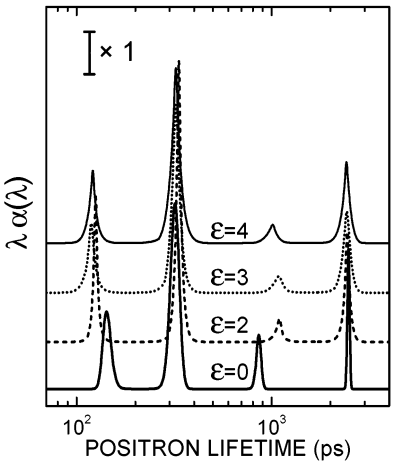

Figure 3. Strain effect on the positron lifetime distribution function for tensile tested UHMW PE. ϵ is the final nominal strain.

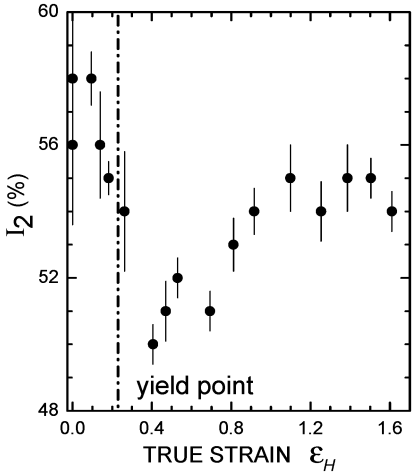

Figure 4. Intensity of the second lifetime peak vs final applied strain for tensile strained UHMW PE.

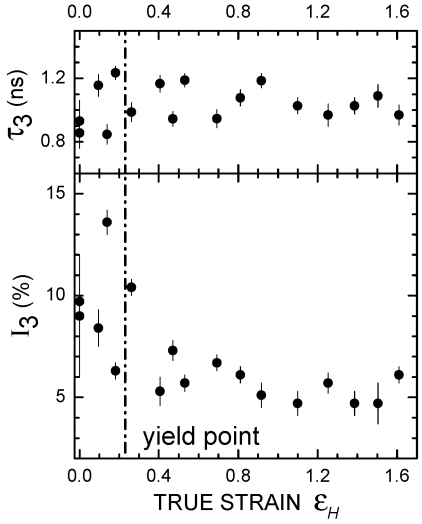

Figure 5. Centroid and intensity of the third lifetime peak, τ_3 and I_3, vs final applied strain for tensile strained UHMW PE.

of the positron lifetime spectra yield lifetimes and intensities in good agreement with the continuous lifetime distribution obtained using the MELT routine. Figure 3 sketches the strain effect on the positron lifetime distribution. The positron lifetime spectra exhibit four well-defined and separated peaks. The peak for the two shortest lifetime components is around 0.130 and 0.320 ns, while the mass centers for the others are found ranging between 0.9 and 1.20 and 2.38−2.50 ns. It is well established that the decay rate of the first lifetime component in a multicomponent spectrum, $\lambda_1 = \tau_1^{-1}$, correlates with the decay rate of the positron state of shortest lifetime by mean of a relation that depends on the kinetics and behavior of the positron and Ps in the material. In a polymer with a four-component lifetime spectrum, (1) the first lifetime component is $\tau_1 \cong 125$ ps/η, where 125 ps is the lifetime of p-Ps in a vacuum and $\eta < 1$ a parameter describing the Ps relaxation in the polymer, and (2) the intensities of the lifetime component have to satisfy the relation $I_1 = (I_3 + I_4)/3$, assuming that the positrons annihilate in free states, p-Ps and o-Ps, via a pick-off process in the crystalline and amorphous phase.[24] In our experiments, I_1 is between 19 and 23% and $(I_3 + I_4)/3$ between 6 and 9%; i.e., I_1 is about 3 times the expected value. Then, the above simple annihilation scheme appears not to be appropriated to describe our experimental spectra. The discrepancy is attributed to an additional short-lived component from a non-Ps state contributing to the p-Ps component.[25] This short component could originate from free positrons because a shorter lifetime is expected for a free positron in the crystalline phase than for a trapped positron or o-Ps. The shortest lifetime peak, arising from *p*-Ps self-annihilation and free positron annihilation in the material, does not provide any relevant information in polymers. The intensity I_1 of our spectra is independent of the applied strain, remaining constant at $I_1 = 21 \pm 2\%$.

The origin of the second lifetime peak centered at 320 ± 20 ps is uncertain. Since free positron annihilation appears to contribute to the shortest lifetime component of the experimental spectra, and the lifetime values of the second component are much shorter than the expected one for o-Ps, it is reasonable to attribute its origin to localized non-Ps positron states. It is hard to elucidate where positrons can be localized or trapped. As probable sites, one would consider (i) the crystalline/amorphous interface, (ii) defects in the crystalline regions, and (iii) holes in the amorphous phase. The variations of the crystallinity and I_2 with final true strain, shown in Figures 2 and 4, indicate that a direct correlation between the second component and the amorphous phase does not exist. Therefore, it appears that e^+ annihilation in holes of the amorphous regions does not contribute significantly to the second lifetime component. We attribute the second lifetime peak to positrons localized at the crystalline/amorphous interfaces, i.e., at the interfacial phase, and at defects in the crystalline lamellae. The initial decrease of I_2, from 58% to a value of 50% when the final applied strain is $\epsilon_H = 0.4$, suggests changes in the interfacial phase induced by the interlamellar slips that occur during the initial deformation stage. Afterward, I_2 increases up to ϵ_H around 1. For ϵ_H above 1, I_2 stays constant, suggesting that some sort of dynamical recovery of defects, or positron trapping saturation in the defects, takes place.

The mass center of the third lifetime peak, τ_3, and the corresponding intensity, I_3, are represented in Figure 5. This third lifetime component with $\tau_3 \sim 1$ ns, observed in PE, is attributed to pick-off annihilation of o-Ps formed in the crystalline phase.[26,27] It has been established that this lifetime τ_3 is correlated with the

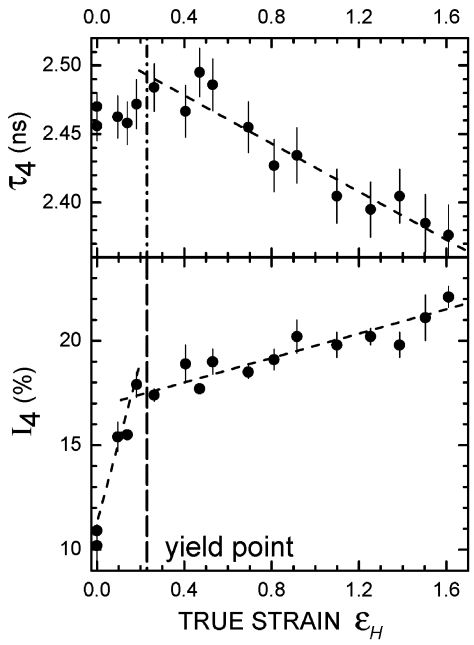

Figure 6. Centroid and intensity of the fourth lifetime peak, τ_4 and I_4, vs final applied strain for tensile strained UHMW PE.

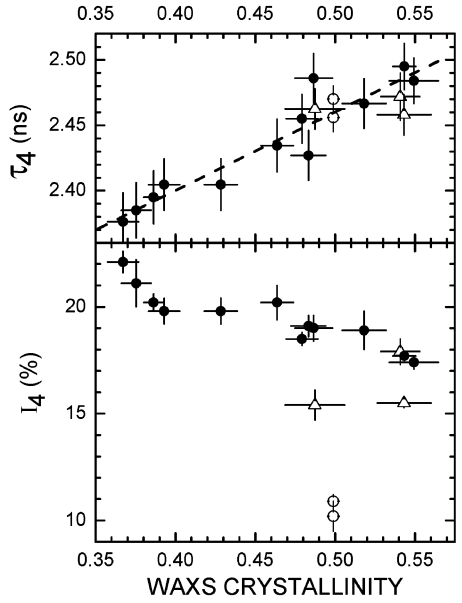

Figure 7. Centroid and intensity of the fourth lifetime peak, τ_4 and I_4, as a function of WAXS crystallinity for tensile strained UHMW PE: (●) strained above the yield point, (△) strained below the yield point, and (○) unstrained.

molecular packing coefficient, C, in hydrocarbon molecular crystals.[25−27] In particular, for PE, Dlubek et al.[26,27] have found that the τ_3 can be fitted to

$$\tau_3 = 7.92 - 9.616C \qquad (4)$$

where τ_3 is given in nanoseconds and C is the volume of the molecule divided by the total volume per molecule. Using the τ_3 values shown in Figure 5, we obtain a mean value for a crystalline packing coefficient of 0.719 ± 0.012. Despite the dispersion of the τ_3 values, this value agrees quite well with the value $C = 0.727$ calculated for PE at room temperature from experimental data in refs 26 and 27. This dispersion is due to an inaccurate determination of the τ_3 values attributable to the weak intensity of the corresponding lifetime component.

A trend of I_3 to decrease increasing strain is observed because of the correlation between I_3 and crystallinity, but the expected decrease of I_3 is not noticeable for $\epsilon_H > 1$. This is could be induced by the fact that part of the third lifetime component might be also due to pick-off annihilation of o-Ps in the solidlike cells which make up the rigid amorphous fraction of the polymer. Such a contribution would be also correlated with the packing coefficient C since these solidlike cells do not contain free volume. The reasons will be make clear in section 3.3 where the results are interpreted in terms of the free-volume model.

The variation of the mass center and the intensity of the fourth lifetime peak with strain are shown in Figure 6. This lifetime component τ_4 is due to o-Ps pick-off annihilation at free-volume local holes.[23,24] The τ_4 value depends, through eq 1, on the size of the free-volume local hole where the positron is localized forming a Ps state, and the intensity I_4 gives us the Ps yield in the free-volume holes of the amorphous phase; i.e., $I_4 = 3P_h/4$, where P_h is the Ps formation probability in the free-volume holes. The results reveal that deformation proceeds increasing the Ps yield in the free-volume holes. During the initial stage of deformation, i.e., up to the yield point, this increase is fast and the size of free-volume holes appears to remain essentially constant as the τ_4 values indicate. For strains above the yield point, the intensity I_4, that is, the Ps formation probability in the free-volume holes, continues increasing at a slower rate, but τ_4 goes down. Above the yield point, τ_4 shows the same strain dependence than the one for the WAXS crystallinity represented in Figure 2, i.e., a linear decrease increasing true strain. Moreover, the crystallinity increase observed in samples deformed below the yield point is correlated with the stage of fast increase in I_4.

Figure 7 represents the variation of τ_4 and I_4 with the WAXS crystallinity. The τ_4 dependence on the crystallinity differs from that found in melt-crystallized PE.[27] τ_4 decreases as the crystallinity diminishes increasing applied strain above the yield point, but τ_4 in melt-crystallized PE decreases increasing crystallinity. However, the decrease of I_4 increasing crystallinity agrees with the results reported for melt-crystallized PE with crystallinities between 3 and 82%.[27] It should be noted that I_4 values for the samples unstrained and strained below the yield point do not follow the same trend than those corresponding to samples strained above, as Figure 7 shows.

The above results indicate two deformation stages which proceed increasing the Ps yield in the free-volume holes of the polymer. The initial stage, which ends up at the yield point, is characterized by a steeply increase of the Ps yield remaining essentially constant of the free-volume hole sizes in the amorphous phase. The second stage produces a continuous increase of the Ps yield in the free-volume holes, apparently lineal up to the fracture, and is accompanied by a decrease of the free-volume hole sizes and a reduction of the crystallinity.

Using eq 1 and the probability density function for the annihilation rate of the fourth lifetime component found by MELT-4, i.e., $\alpha(\lambda_4)$, the probability density function for the free-volume hole radius, $f(R)$, can be obtained. Assuming spherical the free-volume local holes, we can determine the probability density function

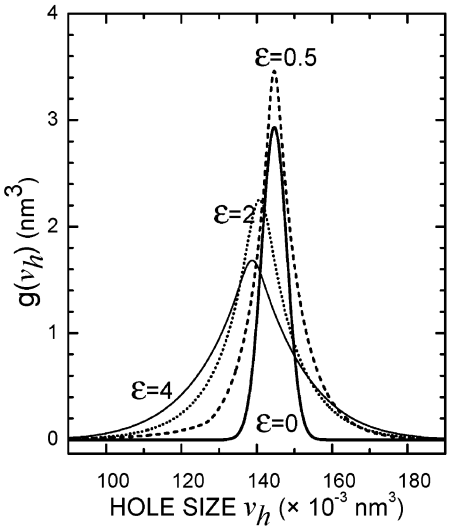

Figure 8. Strain effect on the distribution function of free-volume hole sizes for tensile strained UHMW PE. ϵ is the final nominal strain.

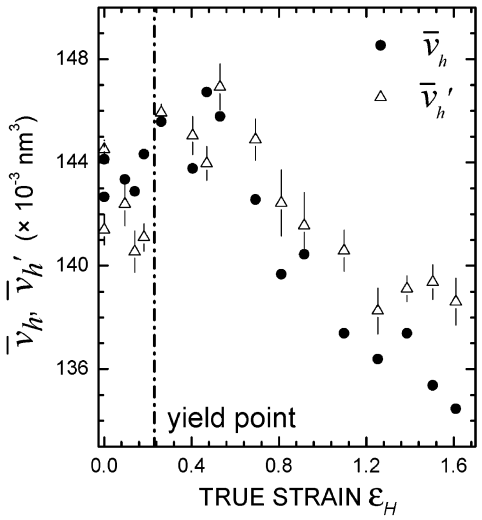

Figure 9. Mean volume of the free-volume holes, $\bar{v}_h$ and $\bar{v}'_h$, as a function of the final applied strain for tensile strained UHMW PE. (●) $\bar{v}_h$ values determined from PALS measurements and (△) $\bar{v}'_h$ values calculated by means of eq 17.

for the free-volume hole sizes, $g(v_h)$, from $f(R)$. It is given by

$$g(v_h) = \frac{f(R)}{4\pi R^2} = -2\Delta R \frac{\cos\left(\frac{2\pi R}{R+\Delta R}\right) - 1}{4\pi R^2 (R+\Delta R)^2 K(R)} \alpha(\lambda_4) \quad (5)$$

where $K(R) = 1 + 8R$ is the correction factor for the Ps trapping rate in the free-volume local holes used by Deng and Jean.[28] Here the hole radius R is given in angstroms.

Figure 8 shows the deformation effect on the distribution of free-volume hole sizes where a positron is localized in the amorphous phase of the samples. This distribution spreads with strain and shifts very slightly toward the smaller volume side increasing strain above 0.5. The mean volume of the free-volume holes probed by the positrons can be obtained using the probability density function $g(v_h)$ by means of

$$\bar{v}_h = \frac{\int_{V_c}^{\infty} v_h g(v_h)\, dv_h}{\int_{V_c}^{\infty} g(v_h)\, dv_h} \quad (6)$$

where V_c represents the minimum hole size in which a Ps atom can form by positron trapping in the amorphous phase of the polymer. The lowest expected value for V_c would be

$$V_c = {}^4/_3\pi(2a_0)^3 = 5 \times 10^{-3}\ \mathrm{nm}^3 \quad (7)$$

Here $2a_0$ is the Ps atom radius (a_0 is the Bohr radius). The $\bar{v}_h$ values vs the final true strain are represented in Figure 9. Although the variations are small, a clear decrease increasing true strain is observed in the strain hardening region, i.e., for true strains above ~0.7.

3.3. Interpretation of the PLS Results in Terms of the Free-Volume Theory. To test our free-volume hole results obtained from positron annihilation measurements, following Liu et al.,[30] we have compared the relative fraction of the cumulative distribution of hole volume $C(v_h)$ calculated by

$$C(v_h) = \frac{\int_0^{v_h} g(v_h)\, dv_h}{\int_0^{\infty} g(v_h)\, dv_h} \quad (8)$$

with the one predicted using a free-volume approach. Following the free-volume model proposed by Grest and Cohen,[29] solidlike and liquidlike cells can be distinguished in the amorphous phase of a polymer. Solidlike cells are those with a volume lower than certain critical value, $v < v_c$, and liquidlike cells those with $v > v_c$. Only the last cells can have associated a free volume that is defined as

$$v_f = v - v_c, \quad v > v_c \quad (9)$$

Positrons in the amorphous phase of a polymer can form Ps atoms annihilating in regions of either high molecular packing or low molecular packing, i.e., in either solidlike cells or liquidlike cells. The annihilation characteristics of Ps in the solidlike cells will be very similar to those in the crystalline phase because both regions have similar molecular packing. Therefore, o-Ps annihilating in solidlike cells would contribute to the third lifetime component. Ps atoms in the liquidlike cells annihilate in free-volume holes associated with these cells. The longest lifetime peak arises from the pick-off annihilation of o-Ps in these free-volume holes as discussed previously.

According to the Grest−Cohen model, the fraction of cumulative distribution of free volume, $C(v_f)$, would be

$$C(v_f) = \frac{\int_0^{v_f} P(v_f)\, dv_f}{\int_0^{\infty} P(v_f)\, dv_f} = 1 - \exp\left(-\frac{v_f}{\bar{v}_f}\right) \quad (10)$$

where $P(v_f)$ is the distribution of free volume in the liquidlike cells given by

$$P(v_f) = \frac{p}{\bar{v}_f} \exp\left(-\frac{v_f}{\bar{v}_f}\right) \quad (11)$$

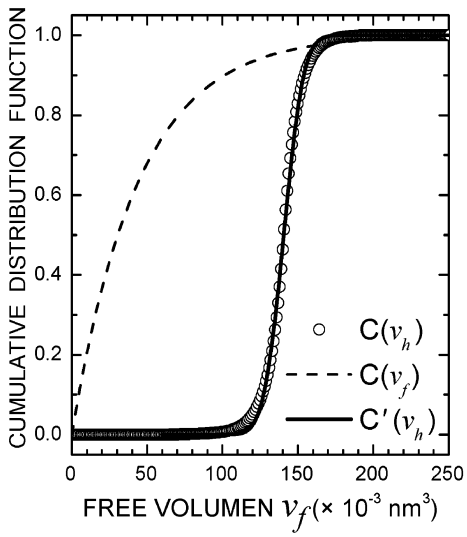

Figure 10. Cumulative distribution function of hole volume $C(v_h)$ obtained from PALS measurements for tensile strained UHMW PE. The curves $C(v_f)$ and $C'(v_h)$ represent the fits of the PALS measurements to the cumulative distribution functions predicted by the free-volume model according to eqs 10 and 16, respectively.

Here, $p = \int_0^\infty P(v_f)\, dv_f$ is the fraction of liquidlike cells, and

$$\bar{v}_f = \frac{\int_0^\infty v_f P(v_f)\, dv_f}{\int_0^\infty P(v_f)\, dv_f} \tag{12}$$

is the mean free volume contained in the liquidlike fraction of the amorphous phase of the polymer.

The $C(v_h)$ data obtained from our results for each deformation experiment, by means of eq 8, are fitted to the cumulative distribution $C(v_f)$ predicted by eq 10 using $\bar{v}_f$ as adjustable parameters. Figure 10 shows the curve $C(v_f)$ obtained for a sample strained up to $\epsilon = 2$. The fit is most unsatisfactory.

In the Grest−Cohen model, the free volume associated with a liquidlike cell, v_f, actually corresponds to the total free volume irrespective of the way it is distributed within the cell. In principle, the free volume v_f can be statistically distributed among holes with different sizes, v_h, where a positron can be localized as a Ps atom. Then, if the corresponding hole size distribution for an unbounded liquidlike cell is denoted by $H(v_h)$, the probability of having a hole with a volume v_h in the polymer should be given by

$$F(v_h) = H(v_h) \int_{v_h}^\infty P(v_f)\, dv_f = H(v_h) p \exp\left(-\frac{v_h}{\bar{v}_f}\right) \tag{13}$$

where $P(v_f)$, given by eq 11, is the probability that a liquidlike cell of the amorphous phase has a free volume v_f. Now, the cumulative distribution function of free-volume hole sizes in the polymer is given by

$$C'(v_h) = \frac{\int_0^{v_h} F(v_h)\, dv_h}{\int_0^\infty F(v_h)\, dv_h} = \frac{\int_0^{v_h} H(v_h) p \exp\left(-\frac{v_h}{\bar{v}_f}\right)}{\int_0^\infty H(v_h) p \exp\left(-\frac{v_h}{\bar{v}_f}\right)} \tag{14}$$

If it is assumed that $H(v_h)$ is a normal frequency distribution given as

$$H(v_h) = \sqrt{\frac{2}{\pi}} \frac{1}{1 + \mathrm{erf}\left(\frac{\langle v_h \rangle}{\sqrt{2}\sigma}\right)} \exp\left[-\frac{(v_h - \langle v_h \rangle)^2}{2\sigma^2}\right] \tag{15}$$

where $\langle v_h \rangle$ is the mean size of the free-volume holes in the liquidlike cell, σ is the full width of the normal distribution function at half-maximum (fwhm), and $\int_0^\infty H(v_h)\, dv_h = 1$, eq 14 gives a cumulative distribution of free volume given by the expression

$$C'(v_h) = 1 - \frac{1 - \mathrm{erf}\left[\frac{\sigma^2 + \bar{v}_f(v_h - \langle v_h \rangle)}{\sqrt{2}\sigma\bar{v}_f}\right]}{1 - \mathrm{erf}\left[\frac{\sigma^2 + \bar{v}_f\langle v_h \rangle}{\sqrt{2}\sigma\bar{v}_f}\right]} \tag{16}$$

The fits of the cumulative distributions $C(v_h)$ obtained from the PLS data to the predicted function $C'(v_h)$ are very satisfactory for all the samples. σ, $\langle v_h \rangle$, and $\bar{v}_f$ are used as adjustable parameters. Figure 10 shows the function $C'(v_h)$ fitted to the data points for the cumulative distribution of the sample strained up to $\epsilon = 2$.

Now, using the distribution function $F(v_h)$ given by eq 13, one can obtained a mean volume of the free-volume holes in the polymer by mean of

$$\bar{v}'_h = \frac{\int_{V_c}^\infty v_h F(v_h)\, dv_h}{\int_{V_c}^\infty F(v_h)\, dv_h} \tag{17}$$

The $\bar{v}'_h$ value for each deformed sample is shown in Figure 9 along with the corresponding value obtained from de PALS measurements through eq 6. The agreement is also very satisfactory. Moreover, the width (fwhm) of the distribution function of free-volume hole sizes obtained from free-volume model, $F(v_h)$, has a strain dependence similar to that found for the distribution function $g(v_h)$ obtained from the PALS data when a liquidlike cell fraction $p = 1$ is assumed eq 13, as shown in Figure 11. The agreement is very satisfactory if $p = 0.65$ is assumed.

The above agreements evidence that the o-Ps states contributing to the longest lifetime component of the polymer probe a distribution of free-volume hole sizes that fits the one predicted by a free-volume approach. Therefore, the fraction of hole volume determined from $g(v_h)$, that is

$$f_h = \int_0^\infty g(v_h)\, dv_h \tag{18}$$

is equivalent to the fractional free volume in the amorphous phase of the samples. The f_h values appear to increase increasing strain as Figure 12 reveals. Initially, the increase is steeply up to a strain around the yield point, i.e., $\epsilon_H \cong 0.23$, coinciding with the initial increase of the crystallinity and I_4 (see Figures 2 and 6). However, coinciding with the strain softening region observed in the stress−strain curve above the yield point, the fractional free volume appears to be insensitive to strain up to the strain hardening onset observed

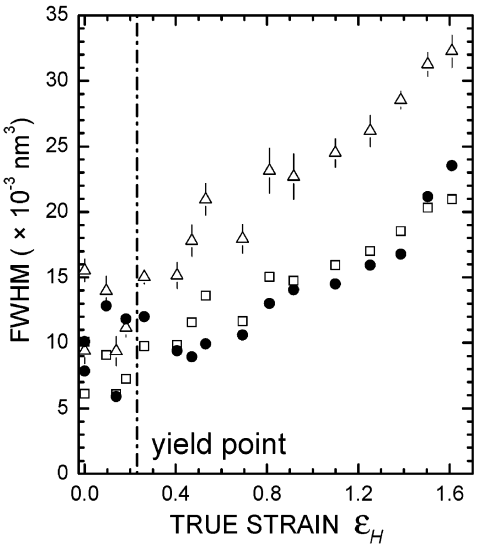

Figure 11. Full width at half-maximum of the free-volume hole size distributions as a function of the final applied strain for UHMW PE. (●) For the distribution function $g(v_h)$ measured by PALS and for the distribution function $F(v_h)$ predicted by eq 13 using (△) $p = 1$ and (□) $p = 0.65$.

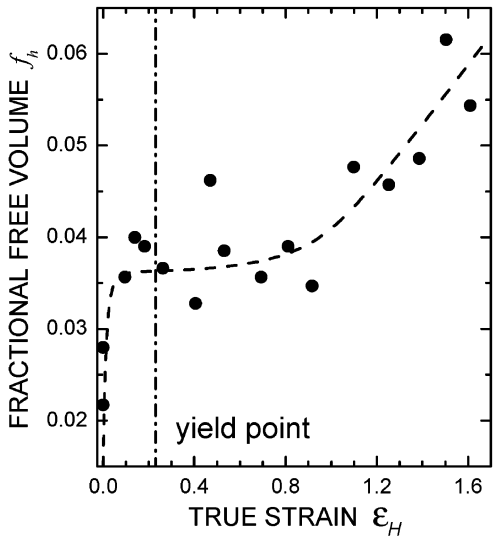

Figure 12. Fractional free volume, contained in the amorphous phase of tensile strained UHMW PE, as a function of the final applied strain.

above ~0.7 of true strain. Above this point, f_h increases continuously with strain up to fracture.

The values obtained for the adjustable parameter $\bar{v}_f$ are shown in Figure 13. It is found that these values increase monotonically for applied strains above the yield point in contrast to the behavior observed for $\bar{v}_h$ in Figure 9.

Since the fraction of amorphous phase in the polymer does not increase for strains up to the yield point, the free-volume increase found below the yield point must be accomplished by structural changes in the amorphous phase. These changes can be (1) the transformation of solidlike cells into liquidlike cells when their local strain results in a cell volume above the critical volume for free-volume formation and (2) the creation of new free-volume holes in the preexisting liquidlike cells. Either mechanism can produce an increase of the o-Ps formation in the free-volume holes increasing the intensity I_4 and the fractional free volume f_h as observed in

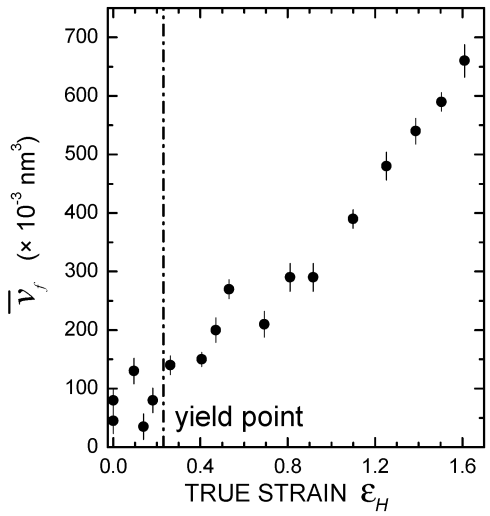

Figure 13. Mean value of the free volume in the liquidlike cells as a function of the final applied strain for tensile deformed UHMW PE. The $\bar{v}_f$ values are obtained from the fits of the PALS measurements to eq 16.

Figures 6 and 12. Mechanism 1 can produce an increase of number of free-volume holes in the polymer without an effective increase of $\bar{v}_h$ and $\bar{v}_f$, while mechanism 2 would induce an increase of $\bar{v}_f$ necessarily. However, the mean size of the free-volume holes and the mean free volume of the cells, $\bar{v}_h$ and $\bar{v}_f$, do not undergo significant changes up to the yield point (see Figures 9 and 13). Thus, the steeply initial increase of the free volume is attributed to mechanism 1.

For applied strains above the strain-hardening onset, i.e., $\epsilon_H \cong 0.7$, $\bar{v}_f$ and f_h increase, and $\bar{v}_h$ and the WAXS crystallinity decrease. Now, the free-volume increase appears to be control by the transformation of crystalline regions of the polymer into amorphous phase and creation of free-volume holes with smaller sizes that the preexisting ones. In addition, small holes must also be formed in the liquidlike cells of the amorphous regions which have not been formed by the crystalline−amorphous transformation. This gives account for the $\bar{v}_f$ increase.

In the strain-softening region, i.e., in the range $0.23 \leq \epsilon_H \leq 0.7$, the variations of the parameters $\bar{v}_h$ and f_h are rather indefinite to extract conclusions.

4. Conclusions

WAXS and PALS measurements performed on tensile deformed UHMW PE reveal correlations between its crystallinity, the positron annihilation characteristics, and the final applied strain to the samples. It is found that the probability of Ps formation in the free-volume holes increases with strain up to failure, and the crystallinity diminishes when the samples are deformed above the yield point.

The size distribution function of the free-volume holes, where a positron is localized and forms a Ps atom, can be determined from their continuous lifetime distribution as well as the fraction of hole volume in the amorphous phase of the polymer. The mean size of the holes decreases when the polymer is deformed in the strain-hardening region but the fraction of hole volume increases.

The results are analyzed in terms of a free-volume approach assuming that the free volume associated with a liquidlike cell of the amorphous phase consists of free-

volume holes whose size distribution is given by a normal frequency distribution. The cumulative distribution functions, determined from the positron annihilation measurements for each deformed sample, are consistent with those predicted by the free-volume approach. This indicates that the positrons contributing to the lifetime component associated with o-Ps annihilation really probe the free volume in the amorphous phase of the polymer. Our experiments shows that tensile strains applied to a polymer can induce free-volume changes unrecoverable after relieving the stress.

Acknowledgment. This research was supported by Consejería de Educación de la Comunidad Autónoma de Madrid (Spain) under the auspices of the Financing Program for the Strategic Groups.

References and Notes

(1) Hiss, R.; Hobeika, S.; Lynn, C.; Strobl, G. *Macromolecules* **1999**, *32*, 4390.
(2) Hobeika, S.; Men, Y.; Strobl, G. *Macromolecules* **2000**, *33*, 1827.
(3) Men, Y.; Strobl, G. *J. Macromol. Sci., Phys.* **2001**, *40*, 775.
(4) Al-Hussein, M.; Strobl, G. *Macromolecules* **2002**, *35*, 8515.
(5) Galeski, G.; Bartczak, Z.; Argon, A. S.; Cohen, R. E. *Macromolecules* **1992**, *25*, 5705.
(6) Bartczak, Z.; Argon, A. S.; Cohen, R. E. *Polymer* **1994**, *35*, 3472.
(7) Bartczak, Z.; Galeski, G.; Argon, A. S.; Cohen, R. E. *Polymer* **1996**, *37*, 2113.
(8) Sha, H.; Harrison, I. R. *J. Polym. Sci., Part B: Polym. Phys.* **1992**, *30*, 915.
(9) Gohil, R. *J. Appl. Polym. Sci.* **1993**, *48*, 1649.
(10) Kobayashi, Y.; Haraya, K.; Hattori, S. *Polymer* **1994**, *35*, 925.
(11) Jean, Y. C.; Yuan, J. P.; Liu, J.; Deng, Q.; Yang, H. *J. Polym. Sci., Part B: Polym. Phys.* **1995**, *33*, 2365.
(12) Compañ, V.; Ribes, A.; Díaz-Calleja, R.; Riande, E. *Polymer* **1995**, *36*, 323.
(13) Hedenqvist, M.; Angestolk, A.; Edsberg, L.; Larsson, P. T.; Gedde, U. W. *Polymer* **1996**, *37*, 2887.
(14) Sodaye, H. S.; Pujari, P. K.; Goswami, A.; Monohar, S. B. *J. Polym. Sci., Part B: Polym. Phys.* **1998**, *36*, 983.
(15) McGonigle, E. A.; Liggat, L. L.; Pethrick, R. A.; Jenkins, S. D.; Daly, J. H.; Hayward, D. *Polymer* **2001**, *42*, 2413.
(16) Monge, M. A.; Villaluenga, J. P. G.; Muñoz, A.; Leguey, T.; Pareja, R. *Macromolecules* **2002**, *35*, 8088.
(17) Ruan, M. Y.; Moaddel, H.; Yu, Z.; Jamieson, A. A,; Simha, R.; McGervey, J. D. In *Positron Annihilation, Proceedings of the 9th International Conference on Positron Annihilation*; Kajcsos, Z., Szeles, C., Eds.; *Mater. Sci. Forum* **1992**; Vols. 105−110, p 1691.
(18) Bartczak, A. S.; Argon, A. S.; Cohen, R. E. *Macromolecules* **1992**, *25*, 5036.
(19) Chu, F.; Yamaoka, T.; Ide, H.; Kimura, Y. *Polymer* **1994**, *35*, 3442.
(20) Nakanishi. H.; Jean, Y. C. In *Positron and Positronium Chemistry*; Schrader, D. M., Jean, Y. C., Eds.; Elsevier: Amsterdam, 1988; p 159.
(21) Murthy, N. S.; Minor, H. *Polymer* **1990**, *31*, 996.
(22) Shukla, A.; Hoffmann, L.; Manuel, A. A.; Peter, M. In *Positron Annihilation, Proceedings of the 11th International Conference on Positron Annihilation*; Jean, Y. C., Eldrup, M., Schrader, D. M., West, R. N., Eds.; *Mater. Sci. Forum* **1997**; Vols. 255−257, p 233.
(23) Kikergaard, P.; Pedersen, N. J.; Eldrup, M. *PATFIT-88*; 1989; RisØ-M-2740.
(24) Mogensen, O. E. In *Positron Annihilation Chemistry*; Springer-Verlag: Berlin, 1995.
(25) Lightbody, D.; Sherwood, J. N.; Eldrup, M. *Chem. Phys.* **1985**, *93*, 475.
(26) Dlubek, G.; Saarinen. K.; Fretwell, H. M. *J. Polym. Sci., Part B: Polym. Phys.* **1998**, *36*, 1513.
(27) Dlubek, G.; Stejny, J.; Lüpke, T.; Bamford, D.; Petters, K.; Hübner, C.; Alam, M. A.; Hill, M. J. *J. Polym. Sci., Part B: Polym. Phys.* **2002**, *40*, 65.
(28) Deng, Q.; Jean, Y. C. *Macromolecules* **1993**, *26*, 30.
(29) Grest, G. S.; Cohen, M. H. *Adv. Chem. Phys.* **1981**, *48*, 455.
(30) Liu, J.; Deng, Q.; Jean, Y. C. *Macromolecules* **1993**, *26*, 7149.

MA049103I